

Chapter 1

Bovine Tail Vertebrae Study

1.1 Introduction

This chapter is split into two main sections discussing initially the development of experimental methods testing bovine tail vertebrae with the second section describing the methods of computationally modelling these vertebrae using FEA@. These main sections are split further into method development, sensitivity tests and the results. In this chapter the experimental and computational work is limited to bovine tail vertebrae due to their plentiful nature and relatively similar geometry to human vertebrae, while not having many of the problems with increased yield strength and density of porcine or other tissue [1]. Allowing translation into using the same or similar methods with human lumbar vertebrae in the following chapter.

1.2 Experimental Methods

1.2.1 Introduction

The experimental methods that have been developed and the early results acquired in this sections allow easier transition to using human tissue and provide valuable results for the development of specimen specific finite element models. Studying these bovine tail vertebrae allows the development of methods for material testing, acquiring μ CT scans of the specimens and carrying out vertebroplasty on the specimens. This is in addition to developing computational models of the vertebrae discussed in section 1.3. The following section will detail the development of various aspects of the experimental procedure, difficulties encountered and traversed, experimental results and finally a discussion of the

methods, results and future work.

The steps involved in the developed methods involve dissection of the soft tissue from the vertebrae, potting in PMMA end-caps, scanning using a μ CT scanner, compression testing and augmentation, the order of which can be seen in fig. 1.1. Specimen preparation, fracture generation and initial μ CT scanning was undertaken jointly with Ruth Coe (PhD student, University of Leeds). Vertebroplasty (following initial training attempts carried out with Dr Peter Loughenbury & Dr Vishal Borse from the Leeds General Infirmary) and subsequent loading and scanning was carried out solely by the author.

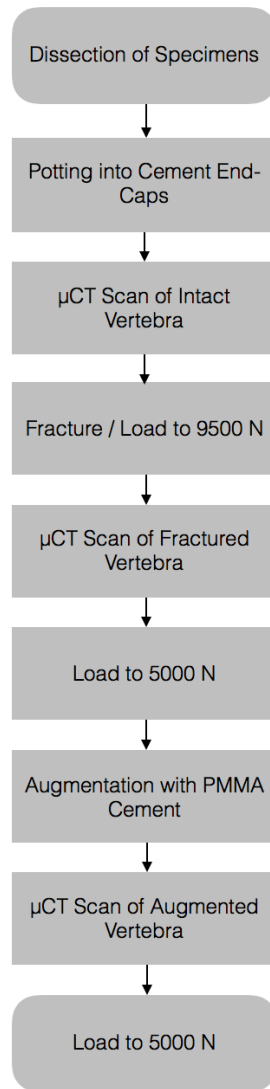


Figure 1.1: Flow-chart detailing the experimental process from initial dissection to final load test.

1.2.2 Specimen Preparation

Bovine tails were acquired from a local abattoir and frozen to -20°C prior to use. They were defrosted in a 4°C fridge for approximately 24 hours before the initial dissection. The three most caudal vertebral (CC1 to CC3) were kept, discarding the remainder of the tail due to the elongation of the vertebral body further distal of the first three vertebrae. In addition to the elongation of the vertebral body the spinal canal narrows limiting its ability to house a steel rod used for mounting the vertebrae in PMMA end-caps. Soft tissue was removed from the vertebrae as thoroughly as possible, including the intervertebral disc material and material occupying the spinal canal. This was carried out in order to remove potential error when comparing experimental results of stiffness to the vertebra models developed from μ CT scans (due to difficulties modelling the soft tissues) and to allow a metal rod through the spinal canal to aid alignment.

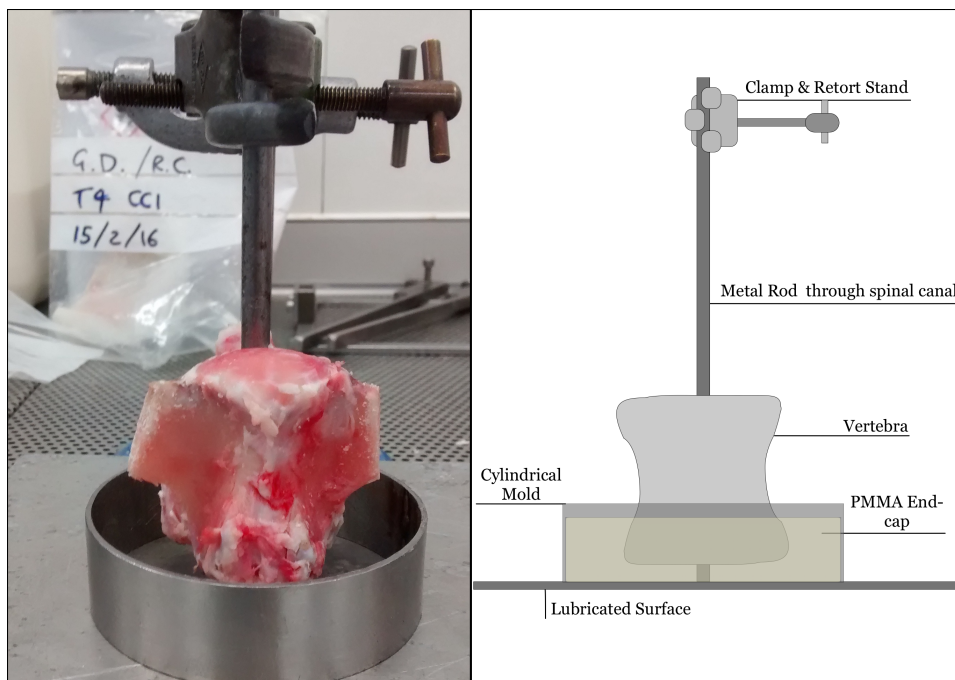


Figure 1.2: Photograph and diagram depicting the method of creating end-caps for the specimens.

Once dissected (and in subsequent breaks between procedure steps) the vertebrae were wrapped in phosphate buffered solution (PBS) soaked tissue, to limit the drying of the vertebral bone. The specimens were potted in PMMA end-caps to allow repeated loading of the vertebrae with the same orientation and positioning, while constraining the vertebrae as little as possible and allowing flexion of the upper endplate. Such flexion (anterior and posterior bending), occurs naturally in the human spine, hence representing this experimentally is important. The setup for potting the vertebrae can be seen in fig. 1.2. Vertebrae were held using retort stands and clamps holding a rod placed through the

spinal canal. Depending on the level of the vertebrae the spinal canal was packed with foam around the rod forming a snug fit while the vertebrae was held approximately 5 mm above a petroleum jelly lubricated metal surface. Also, depending on the level of the vertebrae, any pedicles that protruded past the limits of the metal cylinders were removed with a hacksaw at their base to prevent issues with the loading and scanning tests which followed, most often this was limited to the most caudal vertebrae. The removed pedicles can be seen in fig. 1.2. Lubricated hollow metal cylinders of \sim 10 cm diameter were used to form the endplate when the 2:1 powder to liquid component PMMA mixture was added. PMMA was added until the endplate of the vertebral body was covered up to the point where the body starts to become concave. After approximately 20 minutes the PMMA had sufficiently set to turn over the vertebra and create the end-cap at the other end using the same process with the addition of a level to ensure the creation of parallel end-caps.

Once the PMMA was set the vertebrae were wrapped in more PBS soaked tissue before being frozen or stored in a fridge until the vertebrae were loaded to fracture. The specimens were frozen only if more than 24 hours would pass before the next stage of testing to reduce the number of freeze thaw cycles.

1.2.3 Axial Compression

1.2.3.1 Fracture Creation

All specimens underwent axial compression using a material testing machine in order to generate fractures within the vertebral body. Mounted vertebrae were placed between two steel end-plates, the lower of which contains four screws to inhibit lateral motion of the specimen when under load and the upper plate contains similar screws, with the addition of a chamfered hole. This chamfered hole allows the alignment of the specimen so that the loading point was directly below the head of the testing machine using the marker located above the centre of the vertebral body. The steel ball becomes the centre of rotation for the free to rotate upper end-cap. This permitted rotation mimics natural loading of the vertebrae and increases the likelihood of physiological anterior wedge fractures. Details of the setup can be seen in fig. 1.3.

Loading of the vertebrae starts with a preload from 50 N to 300 N for 10 cycles at a rate of 1mm/minute to remove any viscoelastic effects of any remaining soft tissue. Following the preload, displacement was increased by 1 mm/minute until either the load reached 9500 N (a safety limit due to the 10 kN load cell limit) or a visible failure occurred on the real-time load-displacement plot during compression. This failure was observed as a peak

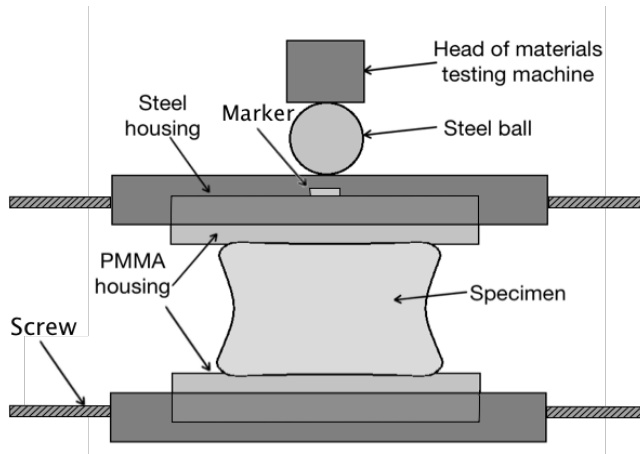


Figure 1.3: The experimental setup for axial loading the vertebral specimens.

in load with the compression being stopped once clear decrease in load was observed. Both scenarios can be seen in fig. 1.4.

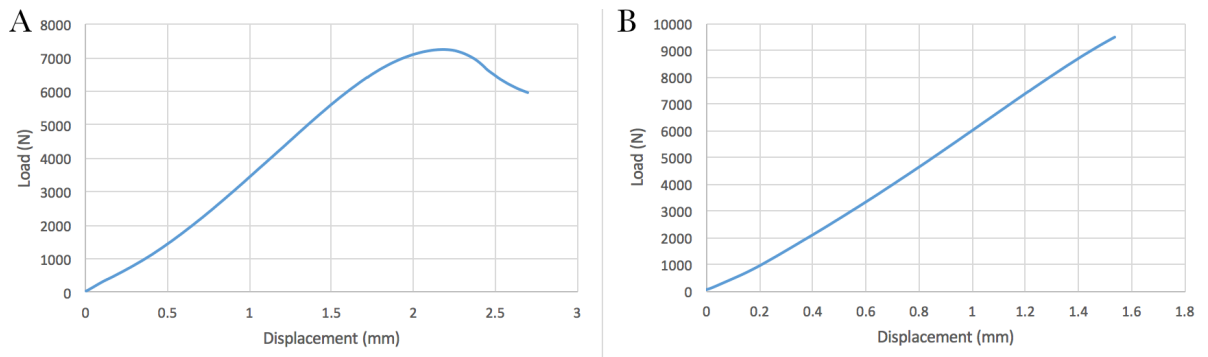


Figure 1.4: The difference between failure (A) and non-failure (B) for bovine tail vertebra compressed to a maximum load of 9500 N or until a peak was observed.

1.2.3.2 Post Fracture & Post Augmentation Loading & Stiffness Calculation

In order to find the stiffness of the previously fractured and augmented specimens a similar loading procedure was used. However, following the preload, compression was stopped when the load reached 5000 N as a means to limit additional damage and fractures to the vertebrae. This ensured that the vertebral stiffness across the three stages (intact, post-fracture and post-augmentation) was calculated from the same range of loads (0 - 5000 N). To examine the effect that the initial load to failure has on the following loads, both post-fracture and post-augmentation, a control specimen was used. This control (T1 CC3) was only loaded up to 5000 N before ending the test.

The stiffness of the specimens throughout their tests was calculated using a Python script on the raw data from the materials testing machine. The script allowed the limits of the

range of interest to be set and, using a defined segment size, incremented over the data reporting the greatest stiffness found in a segment. The segment size was set to 0.3 mm. The script iterated over the data in overlapping increments of 0.1 mm and the range of interest was set to 0 - 5000 N, an explanation of this can be seen in fig. 1.5.

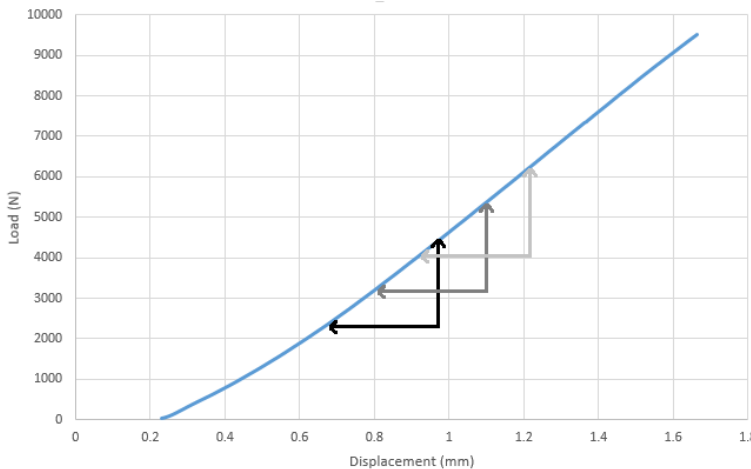


Figure 1.5: A typical load displacement curve showing how the gradient was taken from 0.3 mm long sections incremented at 0.1 mm across the length of the curve.

If the load-displacement curves were perfectly linear within the “linear region” the stiffness in the three ranges of interest in fig. 1.6 (0-1500 N, 0-5000 N and 0-9500 N) would give an equal value for the stiffness or maximum gradient. However, given that these values were found to differ for the three ranges it suggested non-linear behaviour. As shown in fig. 1.6 the recorded maximum stiffness varies greatly depending on what portion of the load displacement graph was being examined. With the maximum stiffness only measurable with the 0-9500 N range. Given that the measured stiffness in the 0 to 5000 N is much closer to the measurement with the full range is included, compared to only including the 0 to 1500 N, it was decided this was a reasonable trade off given the attempt to limit the damage with post fracture tests and the need for a uniform measurement range.

1.2.4 Vertebroplasty

The procedure was developed in collaboration with two clinicians (Dr Peter Loughenbury & Dr Vishal Borse) from the Leeds General Infirmary. Subsequent tests of the procedure were undertaken with the aid of Dr Sebastien Sikora, Dr Fernando Zapata Cornelio & Ruth Coe (Research Fellow, Research Fellow & PhD student respectively), while the specimens presented in the results below were augmented solely by the author.

Due to the differences between human and bovine vertebrae it was not possible to perform bi-pedicular vertebroplasty on the bovine specimens using the methodologies established

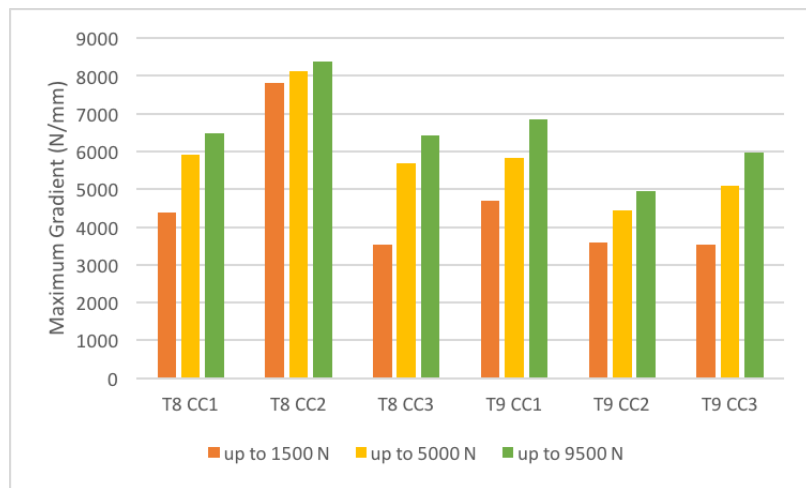


Figure 1.6: The difference seen when measuring the greatest gradient (stiffness) using different portions of the load displacement curve. From 0 to 1500 N, 0 to 5000N and 0 to 9500N.

for human vertebra. The main difficulty was the greatly increased density of the bovine vertebra bone, meaning that rather than pushing the vertebroplasty needle into the vertebra by hand, a mallet and vice to hold the vertebra were required. In addition to this, the force required to inject cement into the vertebral body was greatly increased. The vertebroplasty method for bovine tail vertebra was therefore developed over several iterations due to these difficulties. This sub-section details the initial procedure, the problems encountered and solutions developed to allow a clinically relevant volume of cement to be injected and captured in μ CT scans.

1.2.4.1 Initial Procedure

The procedure was initiated by using bone nibblers to remove the rounded end of both posterior pedicles, providing a surface to start the needle entry. While holding the vertebra in a table mounted vice the needle's 1 cm markings were used to estimate the depth and angle needed to reach the anterior quarter of the vertebral body. The placement of the needle required care to ensure the pedicle was not damaged through splitting as it was inserted. A mallet was used to insert the needle until it was at the depth required; the procedure was repeated for the other pedicle, reusing the same needle.

The PMMA cement was mixed 1:1 monomer to powder to ensure that it could be drawn up via the syringe and to allow enough time to inject the cement before it thickened and set. This additional setting time and reduced viscosity is also used by clinicians, who use ratios up to 0.74 monomer to powder with no adverse outcomes associated despite the reduced modulus and strength often reported [2, 3]. While the vertebra was held in the

clamp of a retort stand, the syringe was attached to the needle, which in turn was inserted into one of the pre-made tracks through the pedicle into the vertebral body. Cement was pushed into the vertebrae using the syringe, until 3-4 mL was inserted into both sides of the vertebrae, with cement being used to back fill as the needle was removed to fill the channel created by the needle. The vertebrae were then left for approximately an hour until the cement had set before scanning.

1.2.4.2 Complications and Changes to the Procedure

Various problems were encountered while carrying out the procedure that required the methods to be adapted. These challenges and their solutions are described below.

Vertebral Temperature: The first of these was the difficulty found injecting any cement into the vertebra. With the initial specimens, cement was injected but it was mainly limited to the needle tracks rather than the vertebral body. To counter this the vertebrae were warmed to 37°C for an hour or until the internal temperature of the vertebrae had reached this temperature (using a temperature probe in the vertebroplasty needle hole). This meant that the bone marrow inside the vertebrae was no longer solid and therefore could be displaced by the cement making the injection much easier.

Radio-opacity of Cement: A second problem was the opacity of the cement on μ CT scans, which proved difficult to segment and separate it from the trabeculae in the vertebral body as can be seen in fig. 1.7:A. Here, the cement was indistinguishable from the bone marrow and can only be seen in the needle channel. The solution to this was to mix barium sulphate (BaSO_4) with the PMMA to achieve the radio opacity seen in fig. 1.7:B, where the bright area in the centre of the vertebral body is the injected cement and BaSO_4 combined. Due to the hydrophilic nature of the BaSO_4 powder it was important to use a completely dry beaker when thoroughly mixing it with the PMMA powder to limit aggregation of the BaSO_4 , which can be seen in the bright spots in fig. 1.7:B. The two components were used in a 1:4 BaSO_4 to PMMA powder ratio, mixed 1:1 with the liquid PMMA component.

Cement Leaking from Vascular Channels: Preventing the cement from exiting the vertebrae from vascular channels while injecting the cement proved to be another obstacle to achieving a physiologic fill volume for the vertebrae. These channels lead both out the anterior face and from the vertebral body into the spinal canal, this can be seen in fig. 1.8 and 1.9. In the body these channels would be filled with vasculature preventing the cement leaking through them. Two main methods were used to stop cement leaking while carrying

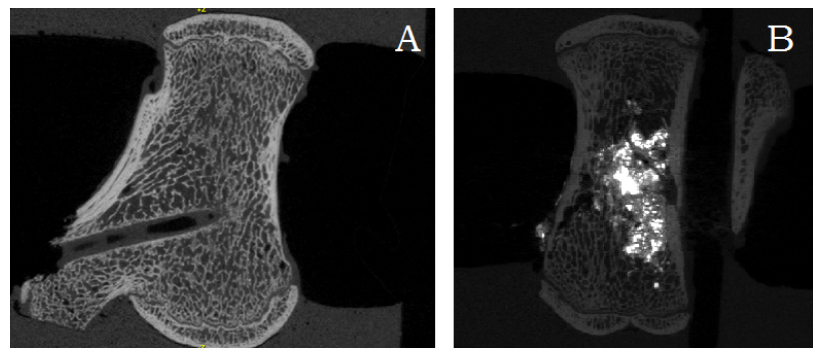


Figure 1.7: A: μ CT scan of an augmented vertebrae, with some visible PMMA residing in the needle channel. B: μ CT scan of an augmented vertebrae using PMMA mixed with barium sulphate.

out the procedure on the bovine tail vertebra. The first was to use the same rod used for mounting the vertebrae in their end-caps to limit the passage of cement into the spinal canal. The second was to use blu-tac to cover the external vascular channels, wrapped with cling-film to hold it in place. This allowed any bone marrow free passage out of the vertebrae, but enough resistance to limit the flow of cement.

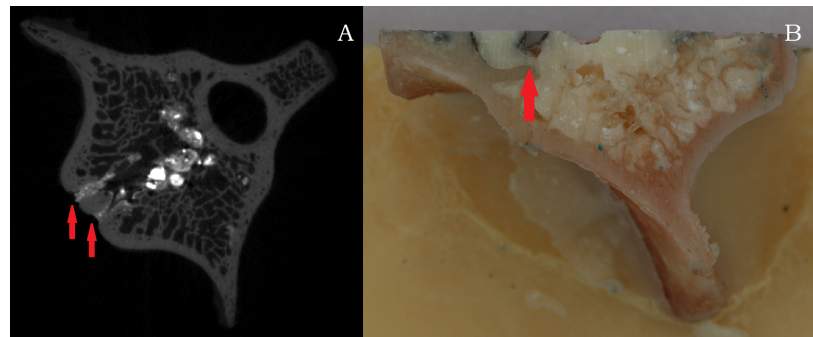


Figure 1.8: A: μ CT scan of an augmented vertebrae showing the cement leaking from vascular channels on the anterior side. B: Photograph of an augmented vertebrae cut into four quarters showing a vascular channel leading into the spinal canal.

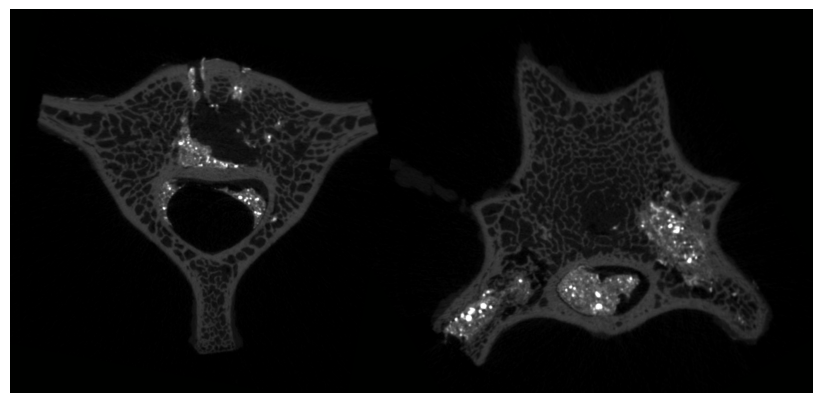


Figure 1.9: μ CT scans of two vertebra, showing the cement leaking into the spinal canal and out of the vascular channels and the vertebral surface.

1.2.5 MicroCT Scanning

μ CT scans were taken at three occasions during the experimental process. These scans occur before and after the initial load to failure, then following the augmentation of the specimens. The process requires the vertebrae to be defrosted and at room temperature, given that the radio-opacity of water differs between solid and liquid states, hence vertebrae were usually defrosted overnight in a 4°C fridge. Vertebrae were loaded two at a time in a carbon fibre loading cradle into a HR-pQCT (XtremeCT, Scanco Medical AG, Switzerland) scanner. The settings used for the scans were: an isotropic voxel size of 82 μ m, energy settings 900 μ A, 60 kVp and 300 ms exposure time. These settings were based upon previous studies using the same scanner and similar vertebrae carried out in the group [1, 4, 5, 6].

1.2.6 Results

The stiffness values for 12 vertebra from 6 bovine tails are shown in fig. 1.10. Of the twelve vertebra only two, the first and second tail vertebra of the second tail (T2 CC1 & T2 CC2), were fractured. The remaining nine (excluding T1 CC3, the control) reached 9500 N and therefore did not fail.

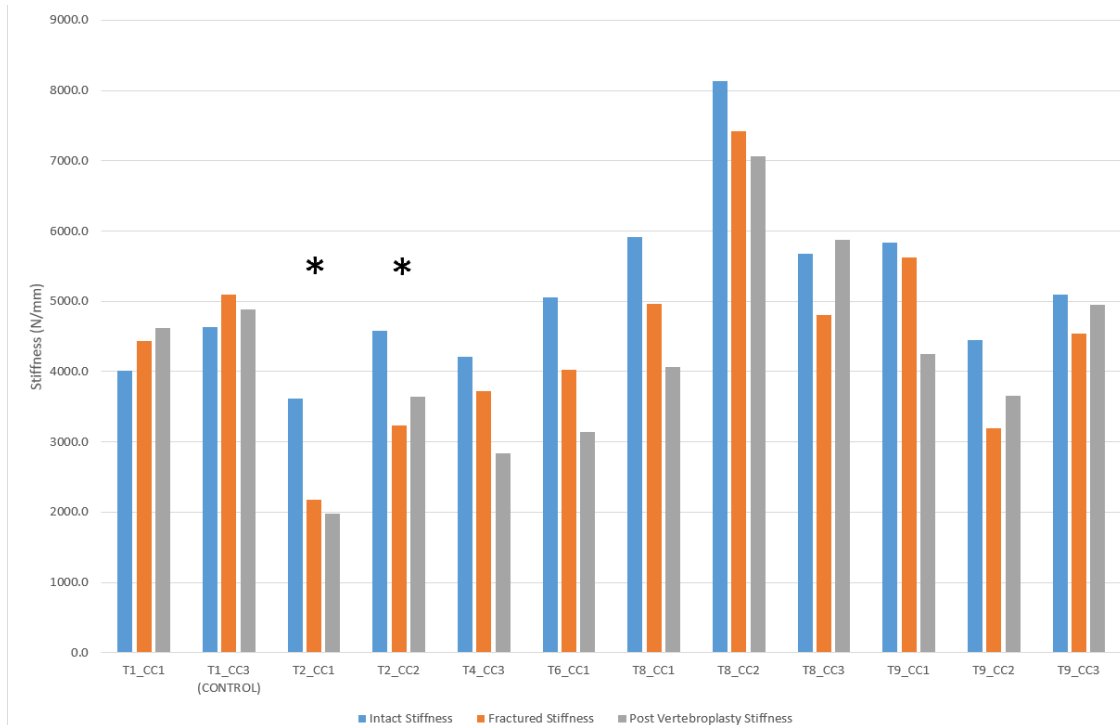


Figure 1.10: The maximum stiffness of 12 bovine tail vertebrae between 0 and 5000 N taken from load - displacement data. Showing the stiffness of the intact vertebrae, a post - fracture stiffness and a post - vertebralplasty stiffness for each. * Indicates those specimens that achieved a clear failure below 9500 N.

The results for the fill volume of cement in the augmented specimens is presented in table 1.1 and was acquired from the down-sampled, segmented models generated from μ CT scans. It shows that fill volume varies between 3% and 17% fill and in addition shows a lack of a correlation between fill volume and increase in augmented specimen stiffness over fractured stiffness with only five vertebrae showing an increase in stiffness. The images in fig. 1.11 shows the extent of the cement fill for the two vertebrae with the largest fill volume.

Table 1.1: The volume of cement and the vertebra volume for the 12 specimens used, along with the percentage cement fill and an indication as to whether the stiffnesses of the augmented vertebrae were greater than the fractured stiffness. This information was measured from the down-sampled models generated from μ CT scans of the vertebrae.

Vertebrae	Cement Volume (mm ³)	Vertebra Volume (mm ³)	Cement Percentage of Vertebra Volume (%)	Increase in Augmented Stiffness over Fractured Stiffness
T1 CC1	2260	32440	6.97	*
T1 CC3	465	27039	1.72	
T2 CC1	663	23285	2.85	
T2 CC2	3405	20373	16.71	*
T4 CC3	1363	25446	5.36	
T6 CC1	830	29332	2.83	
T8 CC1	1257	37357	3.36	
T8 CC2	4489	29248	15.35	
T8 CC3	1041	28403	3.67	*
T9 CC1	2922	45681	6.40	
T9 CC2	2210	38894	5.68	*
T9 CC3	2437	35840	6.80	*

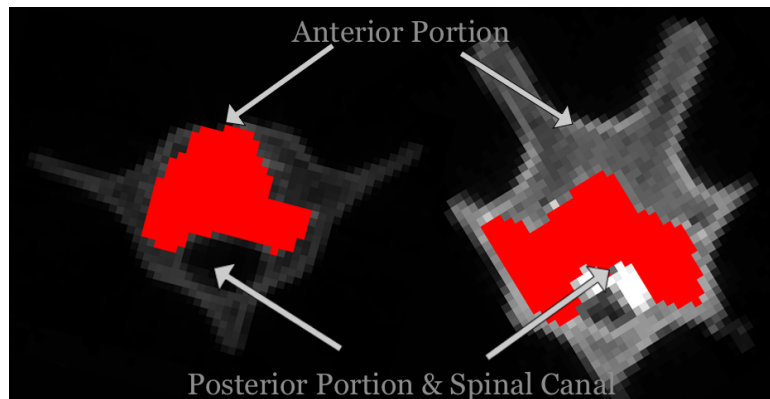


Figure 1.11: Axial μ CT slices of T2-CC2 (left) and T8-CC2 (right), with cement masked in red, showing the extend of cement fill at the point where the cement was most anterior.

The attempt to reduce cement leaking through vasculature during the vertebroplasty procedure can be seen in fig. 1.12. The methods employed greatly reduced the the quantity of cement observed in both the spinal canal and around vascular channels at the vertebral

body surface when compared to scans in fig. 1.9.

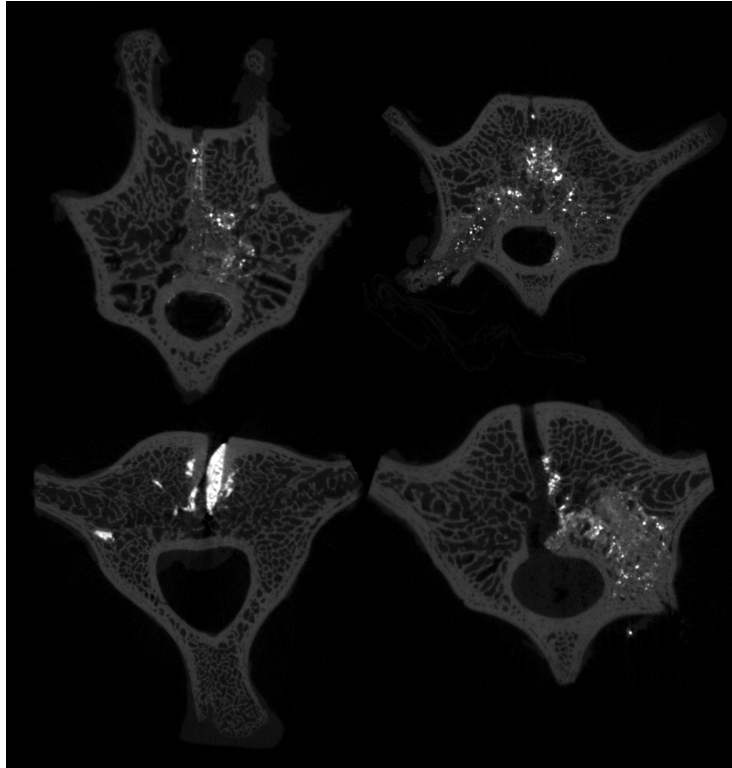


Figure 1.12: μ CT scans of four augmented vertebra using a steel rod to fill the spinal canal and blu-tac to cover the external vascular channels. Shows greatly reduced cement content within the spinal canal with less cement at the surface of vascular channels.

The two plots in fig. 1.13 show a lack of correlation between the difference in stiffness after augmentation when compared to both the fractured and intact specimen stiffness and the intact stiffness. Showing that magnitude of any increase or decrease in the vertebral stiffness following augmentation is not caused, or a feature of the initial, intact vertebral stiffness.

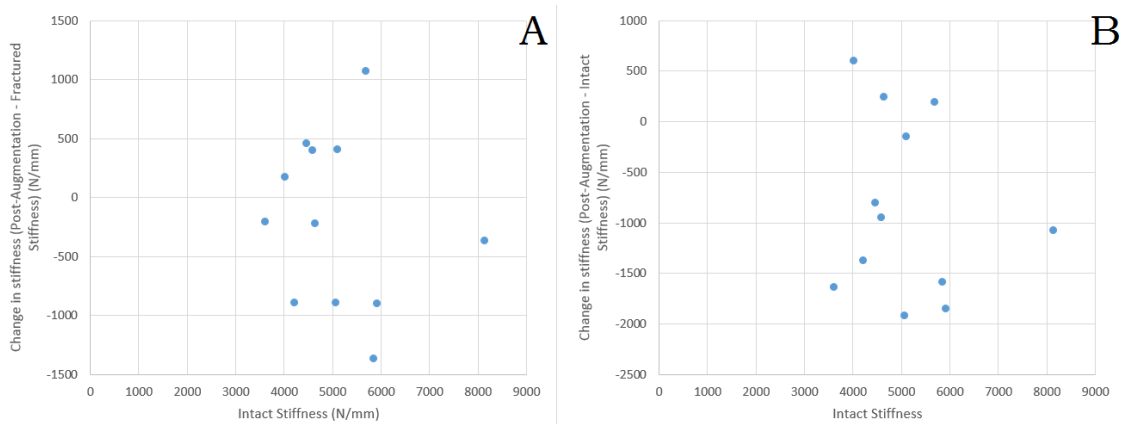


Figure 1.13: A: The difference between the post augmentation and fractured stiffness against the intact stiffness. B: The difference between the post augmentation and intact stiffness against the intact stiffness.

1.3 Finite Element Modelling

1.3.1 Introduction

The finite element modelling of the bovine tail vertebrae, once validated, allows investigations into various properties of the vertebrae and augmentation process. Such investigations include identification of geometric and material property features, which through the use of FE models can be changed programmatically to pinpoint their effects of certain physical scenarios. Scenarios such as vertebroplasty, where the variation can be extended to augmentation procedure variations, potentially leading to suggestions of best practice depending on the properties of the vertebra in question.

Here, the main aim was to develop methods that enable the creation of specimen specific models of bovine tail vertebrae, allowing creation and generation of the much more clinically relevant human lumbar vertebrae using similar methodologies. Initially the focus was on the generation of models that accurately describe the mechanical behaviour of intact bovine specimens, once this was achieved to a reasonable degree an attempt to model augmented specimens was made. In addition to these larger goals, certain sensitivity tests were carried out, including those to understand the effects that additional meshes, mesh sizes and mesh interactions have on model stiffness. Finally some preliminary investigations were made into the effect of changing augmented region positions, however the majority of this investigation will be reserved for ??.

1.3.2 Model Creation

The computational analysis of linear-elastic finite element models was carried out using a combination the segmentation and meshing software, ScanIP (Simpleware, Exeter, UK) and the simulation software, Abaqus (Dassault Systemes, France). The μ CT scans were converted into a finite element mesh using the former software package, this was then imported into the second piece of software to be configured and solved.

The scans acquired from the μ CT scanner were converted from the ISQ file format, generated by the scanner software, into the more portable TIFF image format files using an existing in-house matlab script that additionally converts the greyscale of the scan into 256 bins. This conversion from 16 bit TIFF files with 65,536 bins to 8 bit TIFF files was required due to the limitation to 255 material properties within Abaqus, this allows one greyscale value per material property (assuming all 255 greyscale values are represented in the scan). Once the scan has been pre-processed it was imported into ScanIP ensuring that

the spacing of voxels was correctly set - in this case $82 \mu\text{m}$. Once imported, the location of the loading point was identified to simulate the correct experimental load within ABAQUS; the marker (see fig. 1.3) appears bright on the scan and its centre was taken as the load point, calculated by converting the position into mm. This was achieved by multiplying by the native resolution of $82 \mu\text{m}$.

The following parts of model creation were carried out using a Python script from within the ScanIP software. The script carries out the process described below and was generated by the author by carrying out the process manually and in order to understand the steps required and then writing a script to perform those actions. The development of the script removed much of the user variation in the segmentation of each vertebral model. The effect of user variation during the segmentation process is examined in section 1.3.4.5.

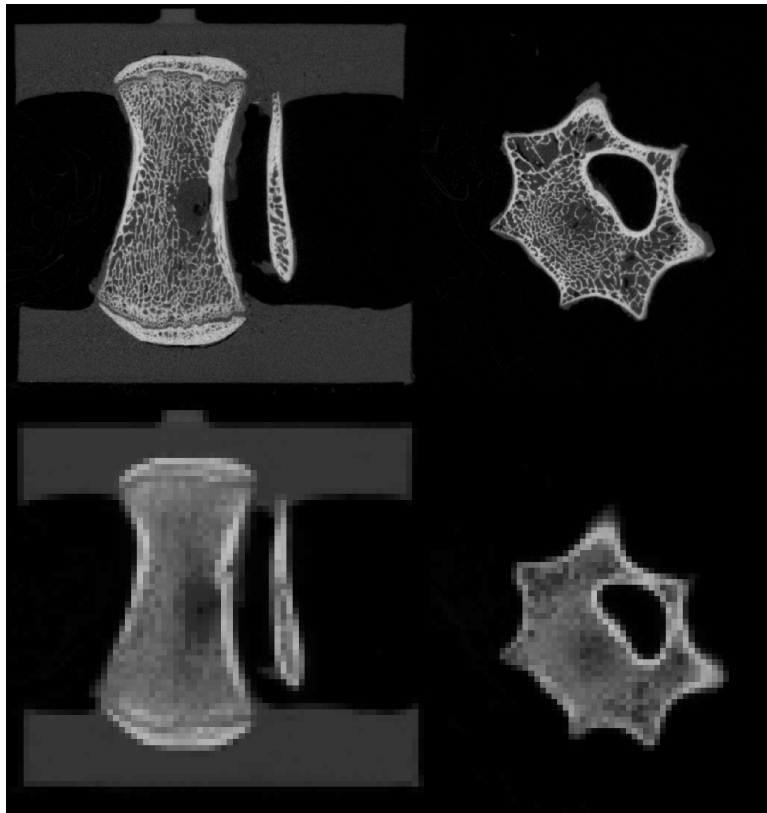


Figure 1.14: Side and top view of a vertebral μCT scan showing the effect of the downsample from $82 \mu\text{m}$ to 1mm cubed.

It was easier to down-sample the image stack prior to segmentation, due to the time required for the software to generate high resolution masks and increased memory usage at higher resolution. The effect of down-sampling can be seen in fig. 1.14. However, in certain cases, for example when modelling vertebral augmentation, in order to attempt to capture the intricacies of the structure and the boundaries between cement and trabecular bone it was favourable to generate the mask prior to down sampling, fig. 1.17. The image stack was down-sampled to voxels 1 mm cubed, due to previous studies producing sensitivity

to mesh size results that showed a good trade off between computational cost and model accuracy [7].

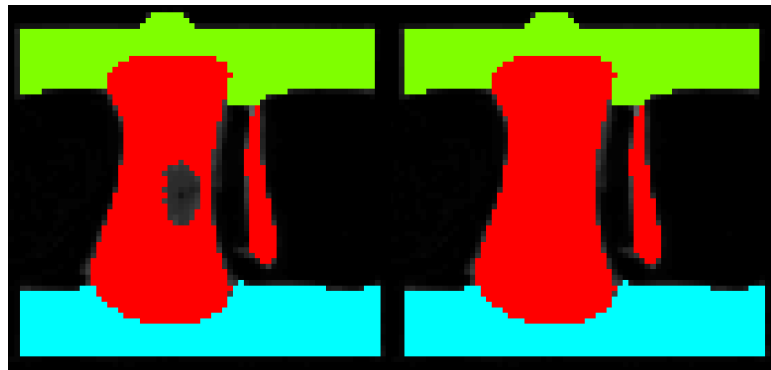


Figure 1.15: Side view of a vertebral model showing segmented vertebra, including the internal void that is filled.

Once down-sampled the image stack was segmented into the constituent parts - the vertebrae and cement end-caps. The different regions that were required to be segmented have different greyscale values, hence the general shape of the masks was created through a thresholding tool that selected volumes of the image stack between two greyscale bounds. For the end-caps these bounds were usually between greyscale values of 12-22 and, if the specimen was not augmented, the vertebrae between 23-255. For augmented specimens these limits change to 23-65 for the vertebrae and 66-255 for internal cement containing barium sulphate. These values were selected by visually limiting the amount of unwanted material selected within the threshold and maximising the wanted material, for example - selecting as much of the end-caps as possible while limiting the selected background and vertebral material to a minimum. This thresholding can be seen in fig. 1.15. It was preferable to avoid internal voids within each mask, due to the potential for errors that may arise from the extra surfaces and contacts created when solved in ABAQUS, these were removed with the use of the morphological close and cavity fill tools within ScanIP (fig. 1.15).

The following parts of the method were carried out manually, following the completion of the automatic segmentation python script. The two end-caps were separated into two separate masks by first duplicating the mask and then flood filling each end-cap to form separate masks.

An FE model was created using the previously generated masks and properties for the volume meshing, materials and contacts were set. The grid size for the model was set to $1 \times 1 \times 1$ using the FE grid algorithm which uses a mix of tetrahedral and hexahedral elements. Material properties were set to homogenous with a Young's modulus = 2.45 (GPa) and Poisson's ratio = 0.3 for the end-caps. Material properties for the internal

cement regions for the augmented vertebrae are described later. The material properties for the vertebral volume were set to a greyscale based material type using the greyscale background information. The coefficients were set so that both the density and Young's modulus were equal to the greyscale value for that element, allowing the Young's modulus to be set correctly in following steps and as described in Section section 1.3.3.

Contacts were set as placeholders to be edited in Abaqus in the steps following. These were contact pairs between each component and another between the superior end-cap and the upper boundary on the Z-axis. The second contact type was a node set between the inferior end-cap and the lower boundary on the Z-axis used to create an enastre boundary condition for the model base.

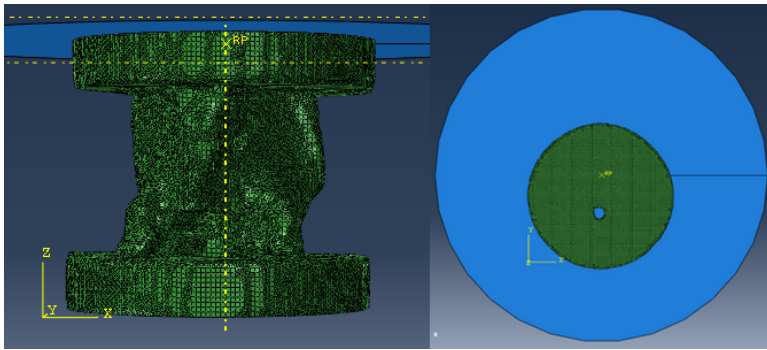


Figure 1.16: Side & top down view of a vertebral model showing the alignment of the analytical rigid plane.

Following this, the FE model was meshed, then exported into an INP file format. This file was imported into Abaqus where the following configuration was completed by a second python script. An analytical rigid plate was created to represent the upper loading platen of the materials testing machine and was centred at the loading point previously found from the marker, this can be seen in fig. 1.16. Once aligned any previous placeholder interactions were removed and a tied interaction was created between the rigid plate and the superior end-cap, along with tied interactions between the vertebra and both end-caps and, if appropriate, to any internal cement volumes. An encastre boundary condition was created at the bottom surface of the inferior end-cap removing all rotational and translational movement and therefore mimicking the experimental setup. A displacement boundary condition was applied to a reference node at the centre of the rigid plate and therefore loading position, the properties were set such that 1 mm of displacement occurs in the negative Z direction; lateral motion in the X and Y planes was restricted, while rotation about the loading point was allowed - mimicking the experimental steel ball setup.

The python script was written to set the material properties of the greyscale dependant vertebral elements by setting the Young's modulus to the greyscale value multiplied by a

conversion factor (which is discussed in section 1.3.3). The script allowed Abaqus to solve the models and outputs the stiffness for each model. This was calculated by dividing the axial reaction force (axis of load application) at the reference point by the 1 mm of displacement.

1.3.2.1 Augmented Model Generation

In order to capture the detail of interdigitation between the vertebrae and the injected cement, the masking process was carried out prior to downsampling, seen in fig. 1.17. If masked post-down-sample it became difficult to define the cement boundaries and the masked volume was inaccurate when compared to the full resolution scan. Masking the internal cement region used the same thresholding approach described above.

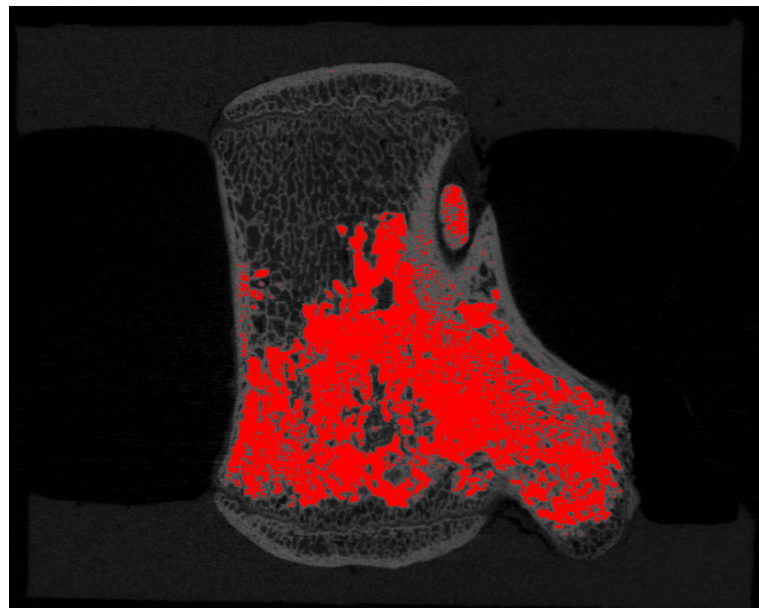


Figure 1.17: A lateral slice through an augmented bovine tail vertebra, showing the cement mask in red at the full $82 \mu\text{m}$ resolution.

1.3.3 Material Properties

1.3.3.1 Bone Material Properties

Material properties for the bone tissue were modelled elastically using a bone element-specific elastic modulus (E_{ele}) that is dependent on the average greyscale value for the element in question (GS_{ele}) with the conversion factor between the two being α .

$$E_{\text{ele}} = \alpha \text{ GS}_{\text{ele}} (\text{GPa})$$

This was required due to each element containing differing quantities of bone and bone marrow due to the continuum level modelling carried out. Hence, a homogenous value for the trabecular bone would not have represented the varying average of material properties seen in each element. The conversion factor, α , was used to convert between the greyscale value for each element and the Young's modulus.

A separate set of 24 bovine tail vertebrae underwent the same experimental and computational methods described previously in order to tune the value of α . This additional set was split into two groups of 12 and was worked on in collaboration with Dr Sebastien Sikora, Dr Fernando Zapata Cornelio & Ruth Coe (Research Fellow, Research Fellow & PhD student respectively). The groups consisted of a calibration group (used to determine the value of α) and a validation group. For the validation group material properties were assigned - multiplying the greyscale for each element by α prior to compressing the model by 1 mm in Abaqus and was used to validate against the experimental values of stiffness.

The calibration for α , the conversion factor was carried out using a golden section search scalar optimisation process. Specifically using the Brent method within the opti4Abq toolbox [8]. The objective of this toolbox was to find the root mean square normalised difference between the experimental specimen stiffness and the finite element stiffness and iterate until the objective function achieved a value of 10^{-3} .

1.3.3.2 Augmented Specimen Material Properties

For convenience the values for the Young's modulus for the interior cement volume were initially set to that of the inferior and superior end-caps. However, from previous studies into modelling bone cement interactions [4, 6, 9, 10, 11, 12, 13, 14], simple material properties of PMMA do not accurately describe the environment. Due to the rule of mixtures and the results found in the literature [9, 15], the effect of reducing the Young's modulus was investigated. This was carried out by reducing the Young's modulus in 10 percent increments from a value of 2.45 GPa to 1.225 GPa.

Additionally, a preliminary investigation was carried out, identifying the effect of a yielding material interface between the bone and the cement, following the work by Sikora [4]. Here, a small interface layer (1 mm in thickness due to the model resolution) represents buckling that occurs in the trabeculae partially captured in the cement volume. This investigation identified the effect of different yield stress values in combination with different Young's moduli for both the interface and the main cement volume.

The yielding region was created through the duplication and then erosion of the cement

mask within Simpleware ScanIP, shown in fig. 1.18. This gave two masks, where one acts as the internal cement volume and the other as an interface layer. Generic material properties were set to the region within ScanIP, allowing the values of the yield stress and Young's moduli values to be changed within the python setup script. The properties tested included changing the yield stress and Young's modulus of the region, whilst maintaining the properties of the internal cement volume at 1.225 GPa. Values for the yield stress in the interface region were varied between 1 MPa and 0.001 MPa, with the material become perfectly plastic beyond this. Young's modulus values for the interface region were varied between 1.225 GPa and 0.1 GPa. These values were manually tuned to find the optimum values with respect to the CCC of the set.

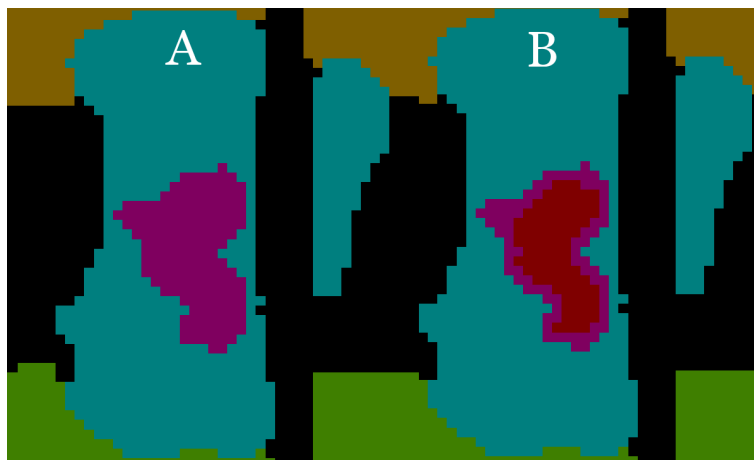


Figure 1.18: Creation of the interface layer: A, showing the initial description of the cement region in pink and B, showing the interface in pink and cement region in red, following the duplication and erosion.

1.3.4 Sensitivity Tests

1.3.4.1 Mesh Size Sensitivity

Element sizes of $1 \times 1 \times 1$ mm were used throughout, following previous convergence studies on porcine vertebrae [7]. The results of the convergence study on porcine vertebrae showed that reducing the element size below $2 \times 2 \times 2$ mm led to changes in the model that were smaller than predicted errors originating from other factors, such as experimental errors and the simplification of boundary conditions. However, reducing the element size to $1 \times 1 \times 1$ mm allows greater resolution when modelling the intricacies of the cement mesh for augmented specimens, the difference between the two resolutions can be seen in fig. 1.19.

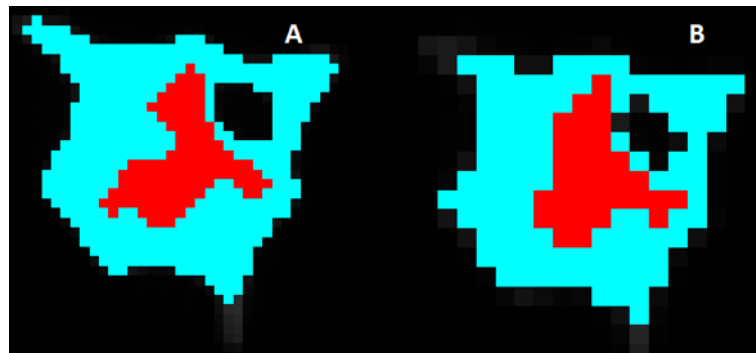


Figure 1.19: Mid-slice through an augmented vertebra, cyan: vertebral body, red: cement. A, element size of $1 \times 1 \times 1$ mm. B, element size of $2 \times 2 \times 2$ mm.

1.3.4.2 Sensitivity to an Additional Mask

The addition of cement into the vertebral body created an extra mesh boundary within the mesh containing the vertebral elements. In order to test what effect this may have on the stiffness of models containing an extra mesh boundary, an un-augmented specimen was tested with an extra mesh representing the cement, but with the material properties of its elements set based on their greyscale as with the other bone elements. The mask was created by duplicating the vertebral mask and eroding it until the volume was approximately 20 % of its original volume. This allowed testing to be carried out on the effect of the extra mesh alone, while using an augmented specimen would allow a more accurate cement shape, it would hinder setting material properties to that of the bone greyscale and create an additional level of uncertainty. Mesh interactions between the two meshes (internal vertebral surface and the cement mask surface) were set using the contact pair interaction and treated similarly to the interaction between the end-caps and the vertebrae. Following model setup in ABAQUS as outlined in section 1.3.2 the model was loaded in compression to 1 mm and its stiffness was recorded.

There was no difference between the two models, with and without the internal cement mesh, meaning that any changes to the augmented model stiffness was due to the material properties of the cement.

1.3.4.3 Mesh Interactions

The effect of mesh interaction between the vertebral body and the internal cement mesh were tested by comparing a) tied interactions between the two surfaces and b) removing any interaction and merely changing the material properties of the internal cement region (neglecting the contact pair steps described earlier). This was carried out for four augmented specimens following the same setup within ABAQUS as described earlier.

The results can be seen in table 1.2, showing a negligible difference between tied and non-tied (single mesh) models. This difference falls well below the difference between experimental and computation, especially for the augmented specimens, hence the effect of this interaction can be neglected from further test.

Table 1.2: The difference between interaction properties, tied and not tied for four augmented vertebrae specimens.

Vertebrae (Tail Number, Vertebral Level)	Tied Interaction (N/mm)	No Tied Interaction (N/mm)	Difference (%)
T2 CC1	5496	5496	0
T2 CC2	8086	8086	0.001
T6 CC1	3686	3686	0.001
T4 CC3	6059	6059	0.0005

1.3.4.4 Augmentation Location Sensitivity

Another preliminary study was carried out (preliminary given the limited nature of the agreement between computational and experimental results and aims to improve this with the use of human tissue) to identify the sensitivity of the models to the position of the cement volume. Tests were carried out to identify the effect of moving a 12 % fill cement volume axially and sagittally in 2 mm increments. This utilised the yielding interface described in section 1.3.3.2 along with the +CAD tools built into Simpleware ScanIP to move a surface based description of the cement volume in the two anatomical planes. A sphere surface of volume equivalent to 12 % fill volume for the T12 CC2 vertebra was created within the +CAD software and imported into the project file for the vertebra, where it was positioned in it's first position. This first position was 1 mm from the top of the vertebral body, ensuring 1 mm of bone surrounded the sphere. It was then converted into a mask, duplicated and eroded in the same method described in section 1.3.3.2 to create the yielding material interface and set with optimum material properties. Following this the mesh was generated and the abaqus input file was exported. The sphere surface was then moved 2 mm in the inferior direction, the previous masks deactivated and the process repeated through the use of a python script to carry out the operations until the bottom of the vertebra had been reached. This was also carried out in the sagittal plane.

The results of moving the cement volumes through the T12 CC2 vertebra are shown in figs. 1.20 and 1.21. For the sagittal plane a reduced stiffness is seen when the volume of cement is positioned most anterially, where the yielding interface of the cement volume encroaches on the denser bone of the cortical shell. Centrally the stiffness is greatest, where

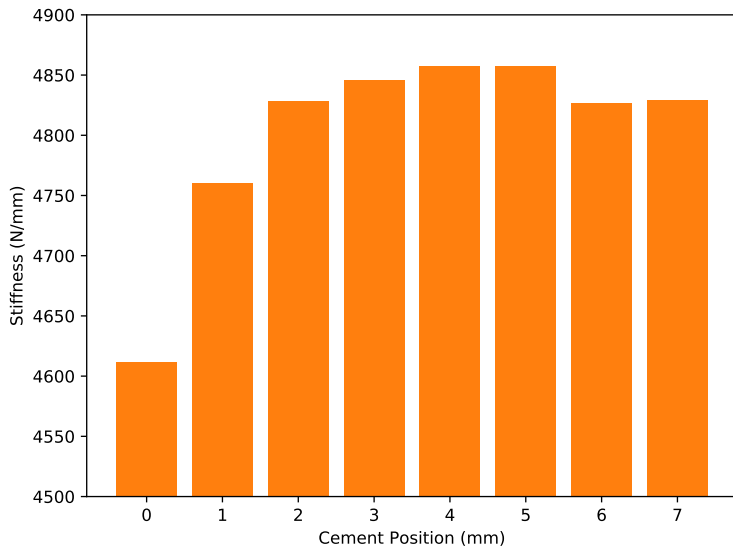


Figure 1.20: The effect of moving the cement volumes from the most anterior position to the most posterior position on the recorded stiffness of the vertebra, when using uniform 12 % fill volume of cement.

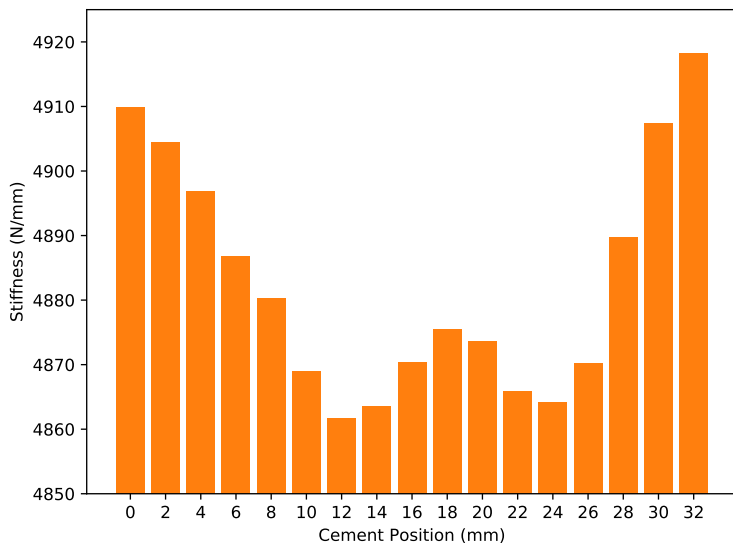


Figure 1.21: The effect of moving the cement volumes from the most superior position to the most inferior position on the recorded stiffness of the vertebra, when using uniform 12 % fill volume of cement.

the cement volume replaces the least dense bone, which can be seen in fig. 1.22, where the least dense (blue) parts are “hidden” by the cement volume in certain positions. Little change to the stiffness at the posterior side of the vertebra is seen due to the additional support from the posterior elements.

Axial movements of the cement volumes show that the most inferior and most superior positions resulted in the greatest stiffness and central positions resulted in the least stiff models. This is potentially due to the greater quantity of bone surrounding the cement volumes at top and bottom where the vertebral body is wider. The peak in the central

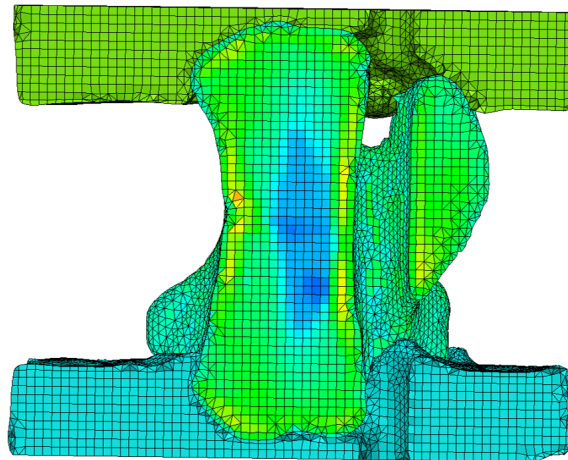


Figure 1.22: A density map of the T12 CC2 vertebra. Yellow/orange elements are the most dense, while blue elements are the least.

loading positions is again likely due to the “hiding” of the weaker bone in the centre of the vertebra.

Finally, despite the changes to the stiffness when moving the cement volume, these changes are smaller than five percent between the most and least stiff result, suggesting cement volume movement at these small volumes is not significant. It may also suggest that cement shape may play a more important role, where endcap to endcap distributions show much larger effects as shown in [11, 16, 17].

1.3.4.5 User Variability Sensitivity

A user variability study was conducted to identify the variation in the modelling approaches, specifically masking the bone and endcap regions. Four users each masked the bone and endcaps for eight vertebrae using thresholding and other morphological filters (which would later be automated using the best approach as described previously). The FE models were then generated and the material properties were optimised using the greyscale optimisation process separately for each users models.

The results for the variability can be seen in table 1.3 showing the mean, maximum, minimum and range as well as the mean for each. The mean range of values was 158, with a mean model stiffness across the four users of 1928 N/mm. The maximum difference between users was for specimen six where a range of 246 was found. This equates to a maximum possible error of 14 % for different users carrying out the same models creation process.

While 14 % error between users if relatively high, the models used in this chapter and

Table 1.3: The variability the modelling approaches of four users with 8 models, each users models undergoing separate greyscale optimisation and FE model solving

Specimen	Stiffness (N/mm)			
	Mean	Maximum	Minimum	Range
1	2457	2567	2379	188
2	2298	2368	2218	150
3	2374	2463	2261	202
4	1600	1659	1545	114
5	2281	2324	2218	106
6	1899	1990	1744	246
7	1330	1398	1236	162
8	1183	1219	1119	100
Mean	1928	1998	1840	158

subsequent chapters were all build by the author. Users tended to produce consistent differences in the stiffness of generated models, for example user one had consistently lower stiffness values and user three had consistently higher stiffness values (means of 1876 N/mm and 1952 N/mm respectively). This, in addition to the fact that the models are built using a python script within Simpleware ScanIP, means that the single user variability should become zero.

1.3.5 Result Analysis

The statistical approach to quantifying the agreement between the computational results and the experimental results for the measured stiffness uses the concordance correlation coefficient (CCC). CCC measures the agreement between two variables and is described by Lin [18] as a method to evaluate reproducibility. The CCC is calculated as:

$$CCC = \frac{2\rho\sigma_x\sigma_y}{\sigma_x^2 + \sigma_y^2 + (\mu_x - \mu_y)^2}$$

Where μ_x and μ_y are the means for the two variables and σ_x^2 and σ_y^2 are the corresponding population variances. ρ is the Pearson correlation coefficient between the two variables. For n independent pairs of samples:

$$CCC = \frac{2S_{12}}{S_1^2 + S_2^2 + (\bar{Y}_1 - \bar{Y}_2)^2}$$

Where,

$$\bar{Y}_j = \frac{1}{n} \sum_{i=1}^n Y_{ij}, \quad S_j^2 = \frac{1}{n} \sum_{i=1}^n (Y_{ij} - \bar{Y}_j)^2, \quad j = 1, 2;$$

and

$$S_{12} = \frac{1}{n} \sum_{i=1}^n (Y_{i1} - \bar{Y}_1)(Y_{i2} - \bar{Y}_2)$$

Specifically, this quantifies the degree to which pairs sit on the $x = y$ line. Departures from this perfect agreement line result in a $CCC < 1$ even in cases where the Pearson correlation coefficient would equal 1. $CCC = 0$ corresponds to no agreement and a value of -1 would be perfect negative agreement.

1.3.6 Results

The optimisation process gave a value for the conversion factor of 0.012529, allowing conversion between greyscale values for elements and their elastic modulus. This value was used for the bone constituents of the intact and augmented vertebrae presented in fig. 1.23, which shows the agreement between the *in vitro* and *in silico* results for the specimen specific models. The agreement of intact vertebrae achieved a concordance correlation coefficient (CCC) of 0.49 compared with 0.14 for the augmented vertebrae (simple tied interaction) (table 1.4). The non-augmented CCC value increased to 0.60 if the uncharacteristically stiff T8-CC2 was removed.

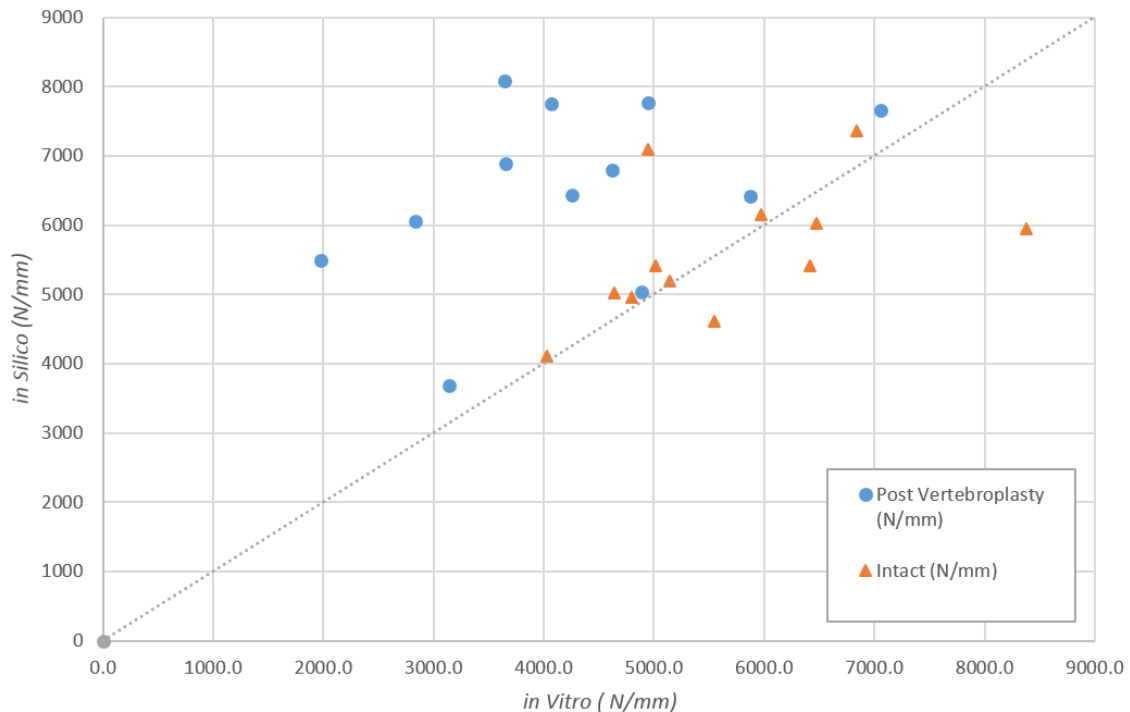


Figure 1.23: The *in silico* compared with *in vitro* stiffness for intact specimens (triangles) and augmented specimens (circles). The dotted line shows a one-to-one correspondence.

Table 1.4: The mean, standard deviation and concordance correlation coefficient (CCC) of the intact and augmented vertebrae (simple tied interaction) for *in vitro* and *in silico* results.

Intact Specimens	Mean Stiffness	Standard Deviation	CCC
<i>in vitro</i>	5684	1196	
<i>in silico</i>	5610	958	0.4895
Augmented Specimens			
<i>in vitro</i>	4246	1371	
<i>in silico</i>	6507	1298	0.14

The effect of changing the modulus of the cement volume in the augmented specimens is presented in fig. 1.24. There was a linear decreases in the stiffness of vertebrae with the reduction of the elastic modulus for the internal cement volume. The two vertebrae that show more prominent decreases in stiffness were those vertebrae that contained larger volumes of cement following their augmentation.

The effect that this has on the data with regard to the *in vitro* stiffness results can be seen in fig. 1.25, where the reduction in *in silico* stiffness moves the data points closer to the $x = y$ line of perfect agreement between the experimental and computational results. This gave a CCC of 0.18.

The increasing agreement with increasing sophistication of modelling the augmentation can be seen in fig. 1.26, comparing the simple tied interaction, the reduced modulus approach and the combination of this and the yielding material interface. The CCC improves when using the reduced modulus at 50 % (1.225 GPa) from the simple tied interaction with an improvement to 0.18 from 0.14. Another improvement is seen when combining the reduced modulus for the cement with the yielding interface (Young's modulus 1.225 GPa, yield stress 0.005 MPa), with the CCC improving to 0.23. The effect of changing these interactions and properties is not uniform, also shown in fig. 1.24, the vertebral models respond differently to different interactions, with increases and decreases seen within the same set of vertebrae when changing the same interaction.

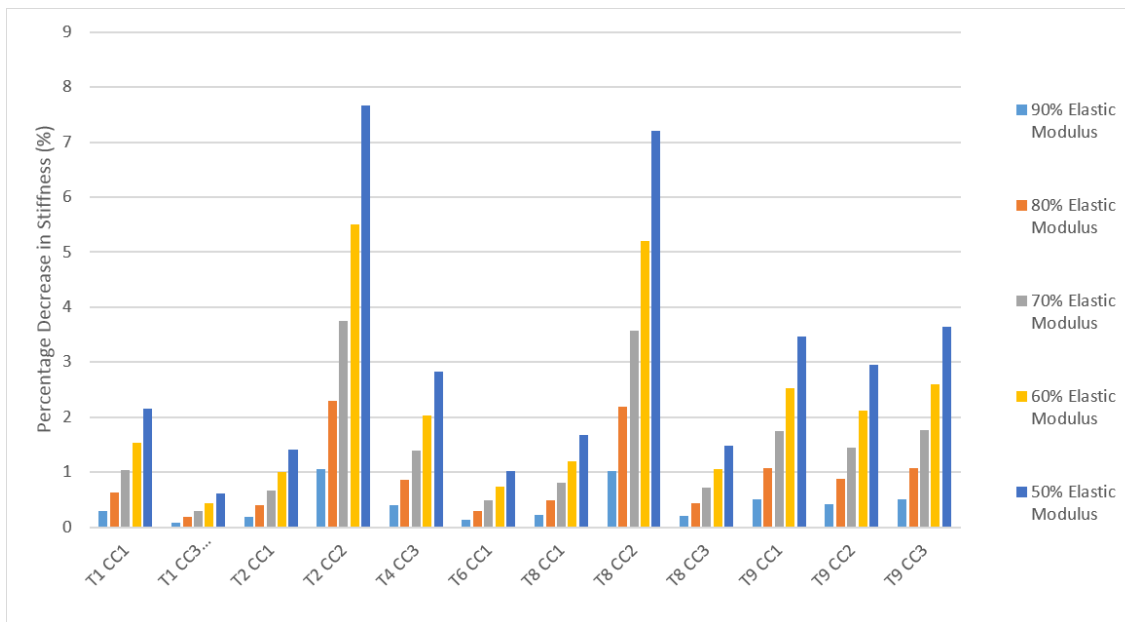


Figure 1.24: The percentage decrease in the vertebral stiffness after reducing the elastic modulus of the cement volume within 12 augmented vertebrae.

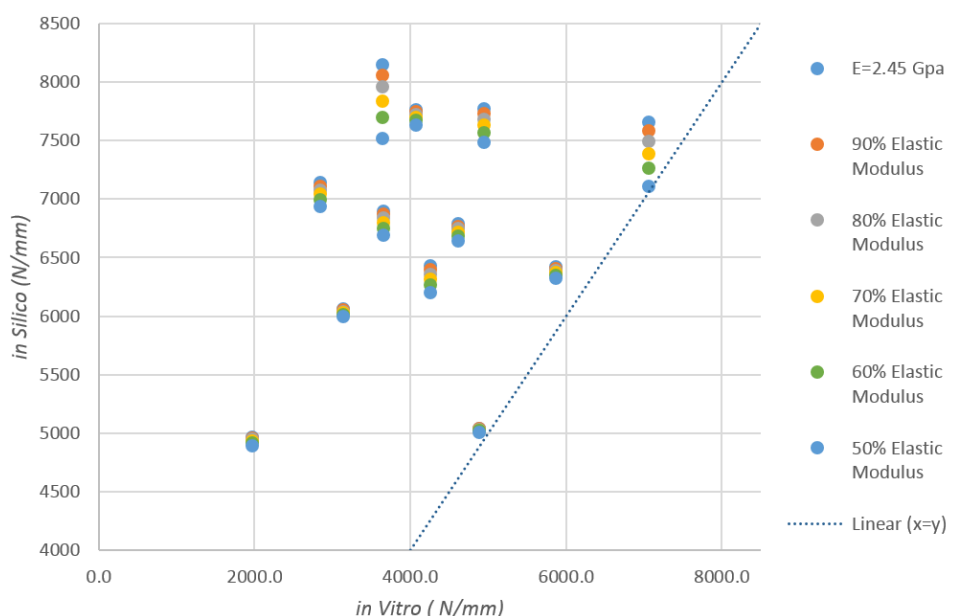


Figure 1.25: The effect of reducing the elastic modulus of the cement volume within 12 augmented vertebrae. Shows the in silico stiffness for the six elastic moduli tested against their in vitro stiffness.

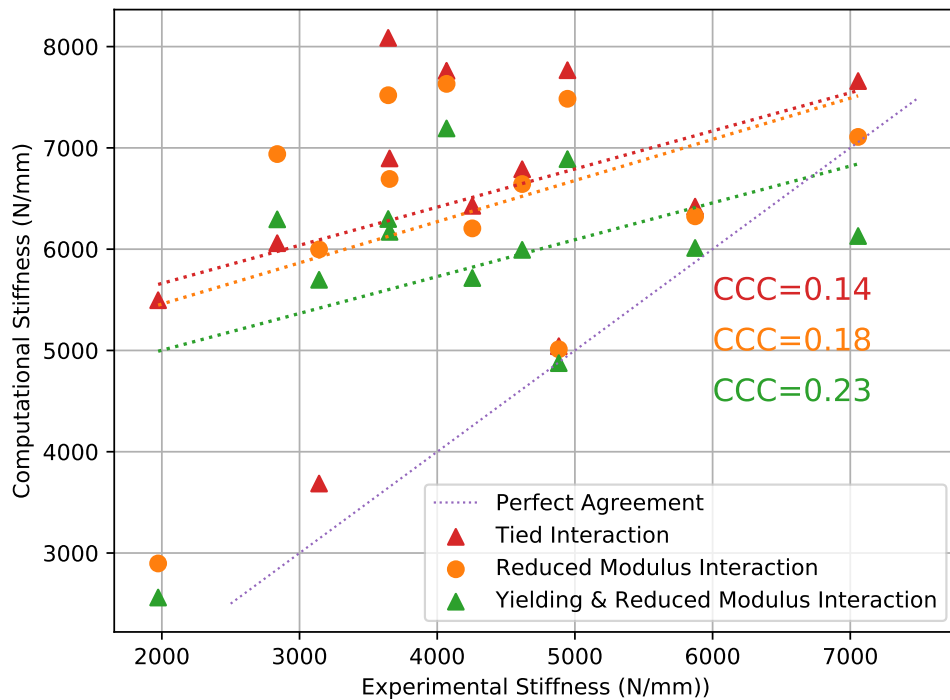


Figure 1.26: A comparison of the different approaches to modelling augmentation in the bovine tail vertebrae. Comparing a simple tie between the bone and cement, a reduced modulus for the cement region and a reduced modulus in combination with a yielding interface layer between the bone and cement.

1.4 Discussion

1.4.1 Experimental Discussion

The experimental section aimed to develop the various aspects of the experimental methodology on a set of bovine tail vertebrae, allowing for an easy transition into using human lumbar vertebrae, which is discussed in the following chapter. Previously developed methods of μ CT scanning have been verified for the bovine tail vertebrae. Methods of performing vertebroplasty and dealing with the unique challenges arising from the bovine vertebrae have been created. The experimental part of this chapter provides a good basis for both the continued modelling of vertebroplasty (especially modelling the cement - trabecular interface) and to continue the experimental work using human tissue. Understanding the challenges of vertebroplasty, will be invaluable when transitioning onto the much more limited source of human vertebrae.

Regarding the results of stiffness at the intact, fractured and augmented stages, the expected trends were not always clear. Most commonly the intact vertebrae have the greatest stiffness with the fractured stiffness showing a reduced value following the damage created with the initial load to failure. The variation of the decrease (and increase) in stiffness for the fractured vertebrae may have a variety of reasons, although the most likely cause is level of damage caused in the initial “load to failure”. These tests varied between the typical load displacement that includes a failure (fig. 1.4:A) and those that show no sign of failure up to the limit of the load cell (fig. 1.4:B). It is difficult to observe any correlation between these vertebra that showed clear failure (T2-CC1 and T2-CC2), those that reached 9500 N and a reduction in the fractured stiffness. It is not to say that the vertebra that reached 9500 N experienced no damage, with the gradient of the load displacement curve often reducing and plateauing as the 9500 N limit approached. The interesting increase in the fractured stiffness for T1-CC1 compared to the intact stiffness may be explained if it is assumed that the compacted trabeculae following the first load to 9500 N result in a stiffer material for the following tests. Other possibilities that may explain the increase in stiffness include a change in the seating of the vertebra within the PMMA endcap. If the initial load changed how the vertebra was positioned in the endcaps it would change the response to loading, even when loaded at the same point.

The cement fill volume information shows that a small percentage of cement is injected into the vertebrae on average, with only two vertebrae approaching the clinically relevant 20% fill. Unexpectedly, only one of these two vertebrae showed an increase in augmented stiffness over the fractured stiffness. A possible explanation is that it is not only the fill

volume that is important in restoring the vertebral stiffness but the placement or shape of the cement fill volumes. This is shown when comparing the segmented scans of the two vertebrae with the greatest fill volume with the T2-CC2 specimen showing cement extending to the anterior wall of the vertebral body, while the cement is limited to the posterior and centre of the vertebral body for T8-CC2. This may help to explain why the stiffness of T8-CC2 did not increase following augmentation. The reduction in stiffness following augmentation for seven of the twelve vertebrae may be due to damage caused by the insertion of vertebroplasty needles. Clinically this damage left behind from the needle channels would heal, most likely restoring the stiffness of the vertebrae back to its intact properties. Additionally, needle insertion into the dense bone of the bovine tail vertebrae required a mallet to reach the anterior portion of the vertebral body, clinically this would not be required due to the much less bone of the human lumbar vertebrae [19]. Such a violent approach would damage the bone surrounding the needle entry, causing micro-fractures not visible on the μ CT scans.

Another possible area of inconsistency is the temperature at which the vertebra were mechanically tested, while it is ensured that the specimens were fully defrosted they were tested at both fridge temperature (4°C) and room temperature (20°C). The effect of this variation in temperature needs to be identified or a consistent temperature needs to be used for subsequent tests.

Despite encouraging results regarding the vertebroplasty methodologies it was difficult to achieve the desired quantity of the cement in the vertebral body. This was mainly due to the difficulty injecting the cement in a smooth manner, which may have been caused by either the tip of the needle becoming blocked following its reinsertion into the needle track, more viscous marrow stopping the displacement of less viscous marrow by the cement or compacted trabeculae around the needle channel that limit the flow of cement past them. One option to test in future work would be side opening needles, which would help guide the cement more accurately to the regions required while circumventing issue with the needle becoming blocked. Additionally, the shape of the vertebrae adds to the difficulty of performing vertebroplasty, with the narrow cylindrical shape of the vertebrae meaning the cement has to travel large distances axially through the trabecular bone to achieve clinically relevant cement fill volumes. In contrast the much wider human lumbar vertebrae used in latter chapters give much more space to inject larger volumes of cement. This, multiplied with a greatly reduced average trabecular density for the osteoporotic human vertebrae (see ?? and [19, 20] should allow for greater volumes of cement to be injected.

When attempting to identify trends between the pre and post augmented and pre and post

fractured vertebral stiffness, no relationships were found. It was expected that initially weaker vertebra would show a larger change in stiffness between the fractured state and the augmented state and similarly between the intact and augmented states. However, no such trends were found, suggesting that properties other than the stiffness or bulk material properties are the cause of the variation. Properties such as the vertebral geometry and trabecular structure, which are investigated through the use of statistical shape models in ??.

The experimental methods currently developed will be of great value when starting experimental work using human tissue albeit many will require adaption due to the differences between the tissue types. These include the density of the bone and methods of inserting the needles, where with the available human tissue being from the elderly, the bones will be most likely be osteoporotic.

1.4.2 Computational Results Discussion

The aims of the computational part of this chapter were to develop methods to build models of vertebrae using automated approaches and to carry out sensitivity tests. These sensitivity tests were to identify the best methods to use when carrying out similar model creation and simulation of the set of human lumbar vertebrae in ?. This was achieved, with automation of the segmentation process within ScanIP and automation of the model setup within Abaqus carried out using a series of python scripts. These scripts require no conversion to be used with the modelling of human lumbar vertebrae, with the exception of the thresholding carried out in scanIP. The preliminary sensitivity tests give a first idea of what variations the vertebrae are sensitive to and will allow further investigation in subsequent chapters.

The computational methods developed and results acquired, as with the experimental results, provide a good base for using human vertebrae and for the continued development of augmented vertebra modelling. The methods and automation of the creation of models both greatly reduce the time spent on model generation and reduce human error. This allows a relatively easy translation to human vertebrae, with only minor adjustments to the thresholds that define materials.

The current methods of masking and meshing the internal volumes of cement in the augmented models provide a good method of creating augmented models. The sensitivity tests carried out on the additional mask inside the vertebrae shows that any effects seen are due to the volume of cement and not a simulation problem. Similarly the

inclusion of a tied interaction between the two meshes failed to affect the result, something especially useful when considering alternative mesh interaction to model the cement - trabeculae interaction. This may be explored further with an expanded sensitivity test identifying whether alternative contacts are more appropriate to model the bone-cement interface.

Augmented volume location sensitivity tests suggests little influence of the position of the cement volume on the reported stiffness when loaded. It does highlight a potential source of error, where anteriorly placed volumes of cement would be expected to increase the stiffness of the vertebrae, given the reduced support and density on the anterior side. However, due to the yielding interface replacing the dense cortical shell, the result is a reduced stiffness. Therefore care needs to be taken when investigating cement volume movement as to not create unnatural simulations. When modelling experimentally augmented models this is not a problem as the cement does not replace the bone when injected, therefore preserving the cortical shell in the vertebral model. Additionally, moving the cement volumes highlights the importance of filling or replacing the weakest, least dense parts of the vertebrae with cement. Although in this case the change of replacing the central “void” in the vertebra is small compared to placing the cement volume elsewhere, as cement volume size increases (and modelling accuracy improves) the effect may become more pronounced. This is investigated further in ??, where cement volumes are moved within statistical shape models of osteoporotic human lumbar vertebrae, which exhibit similarities to the voids found in the bovine tail vertebrae, with much less dense bone in the central portions of the vertebral body.

The intact models agree well with experimental results, with very similar results for the mean and, excluding anomalous results, a good CCC value, showing that the previously validated conversion factor works well with this set of data and that segmentation and model setup works correctly. The poor agreement with the augmented specimen models and their experimental counterparts was an expected result that agrees with similar studies in the literature - [6]. In an attempt to produce a better agreement, the elastic modulus of the cement volume was reduced in accordance with the experimental results of Race et al. [15] and similar methods employed by Wijayathunga et al. [6], where the reduction in modulus is expected due to the greater ratio of monomer to powder used, gaps between the bone and cement and pores within the cement. The reduction in stiffness forms a linear pattern as the elastic modulus is reduced, with those vertebrae that show the greatest reduction being those containing the largest volume of cement. While these results do show a reduction in the stiffness, closer to that of the experimental values, it does not

explain the disagreement fully. This suggests that a combination of improvements to the augmented models are required. The final increase in the agreement between experiment and model was seen with the addition of the yielding interface. This reduced the stiffness of the set on the whole and also increased the CCC value. Interestingly this was not a uniform or predictable effect with no correlation between yielding interface surface area or volume and the change in stiffness. Suggesting the effect was influenced by the density of the surrounding bone on various regions and therefore was not a bulk effect.

Future work will utilise the results acquired, especially those relating to the cement modulus and the cement - bone interactions, to understand how to model this interface more realistically and achieve good agreement between experimental and computation results of stiffness for augmented specimens.

Bibliography

- [1] F. Y. Zapata-Cornelio et al. “Methodology to Produce Specimen-Specific Models of Vertebrae: Application to Different Species”. In: *Annals of Biomedical Engineering* 45.10 (2017), pp. 2451–2460.
- [2] S. M. Belkoff, J. C. Sanders, and L. E. Jasper. “The effect of the monomer-to-powder ratio on the material properties of acrylic bone cement”. In: *Journal of Biomedical Materials Research* 63.4 (2002), pp. 396–399.
- [3] L. E. Jasper et al. “The effect of monomer-to-powder ratio on the material properties of cranioplastic”. In: *Bone* 25.SUPPL. 1 (1999), pp. 27–29.
- [4] S. Sikora. “Experimental and computational study of the behaviour of trabecular bone-cement interfaces.” PhD thesis. University of Leeds, 2013.
- [5] K. Robson Brown et al. “Comparative finite-element analysis: a single computational modelling method can estimate the mechanical properties of porcine and human vertebrae.” In: *Journal of the Royal Society, Interface* 11.95 (June 2014), p. 20140186.
- [6] V. N. Wijayathunga et al. “Development of specimen-specific finite element models of human vertebrae for the analysis of vertebroplasty.” In: *Proceedings of the Institution of Mechanical Engineers, Part H: Journal of Engineering in Medicine* 222.2 (Feb. 2008), pp. 221–228.
- [7] A. C. Jones and R. K. Wilcox. “Assessment of factors influencing finite element vertebral model predictions”. In: *Journal of Biomechanical Engineering* 129.6 (2007), pp. 898–903.
- [8] M. Mengoni. *opti4Abq (v 2.0), a generic python code to run Abaqus in an optimisation loop*. 2017.
- [9] M. Kinzl et al. “The mechanical behavior of PMMA/bone specimens extracted from augmented vertebrae: A numerical study of interface properties, PMMA shrinkage and trabecular bone damage”. In: *Journal of Biomechanics* 45.8 (May 2012), pp. 1478–1484.

- [10] M. Kinzl et al. “The effect of standard and low-modulus cement augmentation on the stiffness, strength, and endplate pressure distribution in vertebroplasty”. In: *European Spine Journal* 21.5 (May 2012), pp. 920–929.
- [11] Y. Chevalier et al. “Cement Distribution, Volume, and Compliance in Vertebroplasty”. In: *Spine (Phila. Pa. 1976)*. 33.16 (2008), pp. 1722–1730.
- [12] S. H. Zhou et al. “Geometrical dimensions of the lower lumbar vertebrae - analysis of data from digitised CT images”. In: *European Spine Journal* 9.3 (2000), pp. 242–248.
- [13] G. Tozzi, Q.-H. Zhang, and J. Tong. “3D real-time micromechanical compressive behaviour of bone - cement interface: Experimental and finite element studies”. In: *Journal of Biomechanics* 45.2 (Jan. 2012), pp. 356–363.
- [14] D. Janssen, K. a. Mann, and N. Verdonschot. “Micro-mechanical modeling of the cement-bone interface: The effect of friction, morphology and material properties on the micromechanical response”. In: *Journal of Biomechanics* 41.15 (Nov. 2008), pp. 3158–3163.
- [15] A. Race, K. A. Mann, and A. A. Edidin. “Mechanics of bone/PMMA composite structures: An in vitro study of human vertebrae”. In: *Journal of Biomechanics* 40.5 (2007), pp. 1002–1010.
- [16] R. Aquarius et al. “Prophylactic vertebroplasty can decrease the fracture risk of adjacent vertebrae: an in vitro cadaveric study”. In: *Medical engineering & physics* 36.7 (2014), pp. 944–948.
- [17] J. Steens et al. “The influence of endplate-to-endplate cement augmentation on vertebral strength and stiffness in vertebroplasty”. In: *Spine* 32.15 (2007), E419–E422.
- [18] L. I.-K. Lin. “A concordance correlation coefficient to evaluate reproducibility”. In: *Biometrics* 45 (1989), pp. 255–268.
- [19] Aerssens et al. “Interspecies Differences in Bone Composition, Density, and Quality: Potential Implications for in Vivo Bone Research”. In: *Endocrinology* 139.2 (1998), pp. 663–670.
- [20] H.-J. Wilke, A. Kettler, and L. E. Claes. “Are sheep spines a valid biomechanical model for human spines?” In: *Spine (Phila. Pa. 1976)*. 22.20 (1997), pp. 2365–2374.